[2] M. K. Scherba and J. E. Rowe, "Characteristics of multisignal and noise-modulated high-power microwave amplifiers," *IEEE Trans. Electron Devices*, vol. ED-18, pp. 11–34, Jan. 1971.
[3] R. W. Laton and G. I. Haddad, "The effects of doping profile on reflection-type IMPATT diode amplifiers," *Proc. 1971 European Microwave Conf.* (Stockholm, Sweden, Aug. 1971), pp. A 5/1:1–A 5/1:4.
[4] E. F. Scherer, "Large-signal operation of avalanche-diode amplifiers," *IEEE Trans. Microwave Theory Tech. (Special Issue on Microwave Circuit Aspects of Avalanche-Diode and Transferred Electron Devices)*, vol. MTT-18, pp. 922–932, Nov. 1970.
[5] W. E. Schroeder and G. I. Haddad, "Effect of harmonic and subharmonic signals on avalanche-diode oscillator performance," *IEEE Trans. Microwave Theory Tech.* (Corresp.), vol. MTT-18, pp. 327–331, June 1970.
[6] M. E. Hines, "Special problems in IMPATT diode power amplifiers," in *1972 IEEE Int. Solid-State Circuits Conf. Dig.* (Philadelphia, Pa., Feb. 1972), pp. 34–35.

18-GHz Paramps with Triple-Tuned Gain Characteristics for Both Room- and Liquid-Helium-Temperature Operation

TORU OKAJIMA, MASAHIKO KUDO, KIYOSHI SHIRAHATA, AND DAIJI TAKETOMI

Abstract—**The design and experimental performance of a wide-band K-band parametric amplifier (paramp) for the experimental domestic satellite communication earth station are described. An optimum idler frequency for a minimum noise temperature is derived taking into account the varactor diode skin effect. Wide-band paramps with a double-tuned signal circuit are discussed and it is shown that triple-tuned gain characteristics are realizable with this configuration. Finally, an 18-GHz paramp is described, which can be operated from room- to liquid-helium (LHe) temperature, only requiring adjustment of pumping power and bias voltage and using lithium ferrite circulators. Triple-tuned gain characteristics with a bandwidth of 1300 MHz at a gain of 10 dB are obtained using a miniature pill prong packaged varactor.**

I. Introduction

THE PAPER describes the design and experimental performance of a wide-band K-band paramp with both cryogenically cooled and room-temperature operation and intended for use in experiments on domestic satellite communication.

As the signal frequency is at K band and the idler frequency is in the millimeter wave region, skin effect in the varactor diode cannot be ignored, and the results obtained by Greene and Sard [1] must be modified.

A design technique to maximize the voltage gain-bandwidth product of a single-tuned paramp has been presented [2]. Design techniques on paramps with a double-tuned signal circuit have been also represented by DeJager [3] and Connors [4], and conditions to obtain maximally flat gain characteristics have been included therein. However, these conditions are restrictive in that the paramp gain cannot be chosen at will after other parameters of the paramp have been established. Getsinger [5] has presented the requirements on second signal resonator Q for obtaining wide-band gain characteristics as a function of the gain ripple and the single-tuned bandwidth. Because an equivalent circuit of single-tuned paramps cannot always be entirely represented by a negative resistance and positive reactance elements, these results are sometimes difficult to apply.

Broad-band matching of a parametric amplifier by the network synthesis method has been presented by Porra and Somervuo [6]. But this paper intends to derive the broad-banding factor, the shape of the resulting gain characteristics, and the required Q of the second signal resonator for paramps with a double-tuned signal circuit in terms of given single-tuned paramps.

The required noise temperature for a K-band paramp system is about 100 K based upon the antenna noise temperature considerations. This noise temperature

Manuscript received May 15, 1972; revised July 24, 1972. This paper was presented at the 1972 International Microwave Symposium, Chicago, Ill., May 22–24, 1972.

T. Okajima is with Musashino Electrical Communication Laboratory, Nippon Telegraph and Telephone Public Corporation, Musashino City, Japan.
M. Kudo is with the Microwave Division, Nippon Telegraph and Telephone Public Corporation, Tokyo, Japan.
K. Shirahata and D. Taketomi are with Kamakura Works, Mitsubishi Electric Corporation, Kamakura City, Japan.

level can be obtained with a 2- or 3-stage liquid-nitrogen cooled paramp. However, it is considered to be more useful to realize the overall system as a combination of paramps operating at room and cryogenically cooled temperatures, as will be discussed herein.

Accordingly, the characteristics of an 18-GHz low-noise amplifier system for the experimental domestic satellite communication earth station consisting of a 1-stage liquid-helium-cooled paramp and a 2-stage room-temperature paramp will be presented.

II. Optimum Idler Frequency

An optimum idler frequency which minimizes noise temperature can be derived in terms of the dynamic Q, $(\tilde{Q})$, of the varactor diode [7]. But at frequencies above about 20 GHz, skin effect in the varactor diode cannot be ignored so that its series resistances R_{S1} and R_{S2} at the signal and idler frequencies, f_1 and f_2, are not equal. Therefore, it is reasonable to derive an optimum idler frequency, defining the ratio of the dynamic Q at the signal frequency to that at the idler frequency as given in

$$\frac{\tilde{Q}_2}{\tilde{Q}_1} = \frac{f_1}{f_2}\frac{R_{S1}}{R_{S2}} \fallingdotseq \frac{f_1}{f_2}\left(\frac{f_1}{f_2}\right)^{1/m}, \qquad (m = 2 \sim 3). \tag{1}$$

Here, f_1 and f_2 represent the signal and idler frequency, respectively. Theoretical and experimental bases for (1) are given in the Appendix.

Furthermore, the noise temperature rises as the signal frequency deviates from the signal center frequency, so that the aforementioned condition for the minimum noise temperature at the signal center frequency may be modified to yield that at the signal band edges.

A noise equivalent circuit for paramps is shown in Fig. 1. Current in the idler circuit i_2 is given by

$$i_2 = -\frac{e_{n2} + j\tilde{Q}_1 R_{S1} i_1^*}{R_{S2} + jX_2}. \tag{2}$$

Voltage induced in the signal circuit by this current is $j\tilde{Q}_2 R_{S2} i_2^*$ and

$$j\tilde{Q}_2 R_{S2} i_2^* = -\frac{j\tilde{Q}_2 R_{S2} e_{n2}}{R_{S2} + jX_2^*} - \frac{\tilde{Q}_1\tilde{Q}_2 R_{S1} R_{S2} i_1}{R_{S2} + jX_2^*}. \tag{3}$$

Hence the noise equivalent circuit at the signal frequency can be shown in Fig. 2. Consequently, an exchangeable noise power P_e can be represented as the mean-squared open-circuited noise voltage at the signal circuit divided by 4 times the real part of the impedance at that terminal,

$$P_e = \frac{\bar{e}_{n1}^2 + \bar{e}_{n2}^2 \left|\dfrac{j\tilde{Q}_2 R_{S2}}{R_{S2} - jX_2}\right|^2}{4\left[R_{S1} + R_e\left(-\dfrac{\tilde{Q}_1\tilde{Q}_2 R_{S1} R_{S2}}{R_{S2} - jX_2}\right)\right]}. \tag{4}$$

A noise figure of the paramps at the large-gain condition

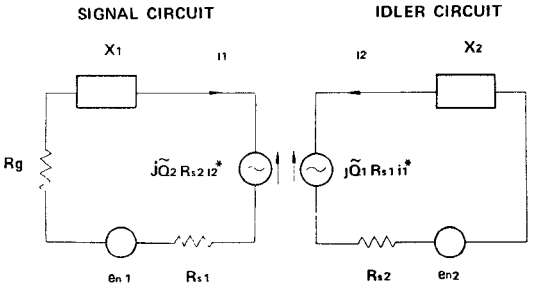

Rg : GENERATOR RESISTANCE
i : CURRENT
X : REACTANCE
e^2_{n1} = 4KTBRs1
e^2_{n2} = 4KTBRs2
K : BOLTSMAN'S CONSTANT
T : TEMPERATURE
B : BANDWIDTH

Fig. 1. Paramp noise equivalent circuit.

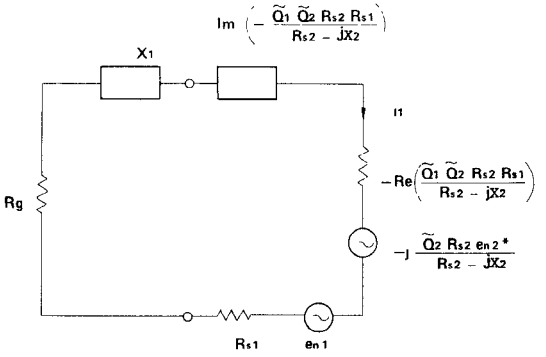

Re : REAL PART, Im : IMAGINARY PART

Fig. 2. Paramp noise equivalent circuit at signal frequency.

F is given by [8]

$$F = 1 + \frac{-P_e}{kT_0B} = 1 + \frac{T}{T_0}\cdot\frac{\tilde{Q}_2^2\left(\dfrac{R_{S2}}{R_{S1}}\right) + 1 + \left(\dfrac{X_2}{R_{S2}}\right)^2}{\tilde{Q}_1\tilde{Q}_2 - 1 - \left(\dfrac{X_2}{R_{S2}}\right)^2}. \tag{5}$$

Here, T_0 is 290 K. X_2/R_{S2} in (5) can be rewritten as follows by introducing (1):

$$\frac{X_2}{R_{S2}} = 2Q_{u2}\frac{\Delta f}{f_2}\cdot\frac{R_{S1}}{R_{S2}} \fallingdotseq 2d_2\frac{\tilde{Q}_1}{\gamma/2}\cdot\frac{\Delta f}{f_2}\cdot\left(\frac{f_1}{f_2}\right)^{1+(1/m)} \tag{6}$$

where

Q_{u2} Q of the idler circuit (not considering skin effects of varactor diodes),

$Q_{1,2}$ Q of a varactor diode at the signal frequency and the idler frequency, respectively,

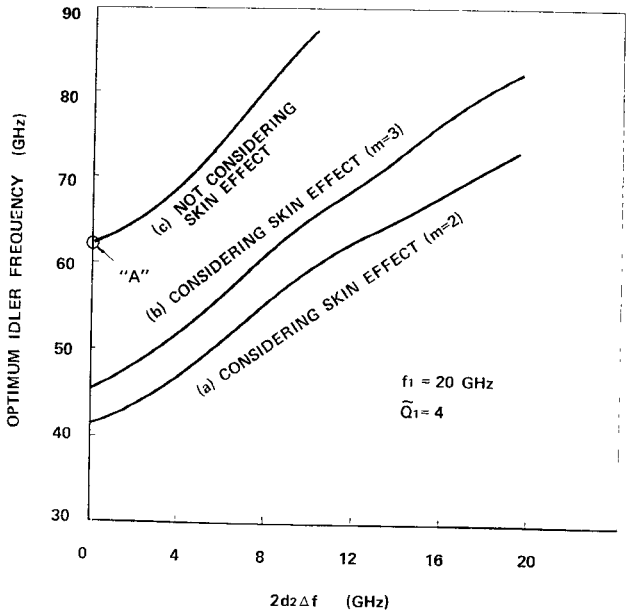

Fig. 3. Optimum idler frequency for minimum noise performance versus signal bandwidth, including consideration of skin effect.

$2\Delta f$ bandwidth,
$\gamma/2$ diode pumping factor $\equiv 0.25$,
d_2 $= Q_{u2}/Q_2$ (slope factor).

Using (1) and (6), (5) becomes

$$F = 1 + \frac{T}{T_0} \cdot \frac{\left(\frac{f_1}{f_2}\right)^{1+(1/m)} - \frac{1}{\tilde{Q}_1^2} + \left[8\left(\frac{f_1}{f_2}\right)^{1+(1/m)} \cdot \frac{d_2\Delta f}{f_2}\right]^2}{\left(\frac{f_1}{f_2}\right)^{1+(1/m)} - \frac{1}{\tilde{Q}_1^2} - \left[8\left(\frac{f_1}{f_2}\right)^{1+(1/m)} \cdot \frac{d_2\Delta f}{f_2}\right]^2} \cdot \quad (7)$$

Assuming $\tilde{Q}_1 = 4$, $f_1 = 20$ GHz, and $T = T_0$ in (7), the optimum idler frequency for minimum noise figure is presented in Fig. 3, as a function of $d_2\Delta f$ for no skin effect and for skin effect exponents $m = 2$ and $m = 3$, respectively. These results show that the optimum idler frequency in the presence of skin effect is lower than that in its absence. For a particular example, if $2\Delta f = 1.0$ GHz and $d_2 = 3$ are assumed, the optimum idler frequency in the presence of skin effect will be 45 GHz for $m = 2$ and 50 GHz for $m = 3$.

Ambient temperature increases caused by pump heating must also be considered in determining the optimum idler frequency. It has been shown that this contribution further decreases the optimum idler frequency since the required pump power is proportional to the square of a pump frequency f_p [9].

As shown in Section V, it is desirable to choose the idler frequency at the parallel resonance of the varactor diode in order to maximize the bandwidth.

III. Gain-Bandwidth Characteristics of Paramps with Double-Tuned Signal Circuits

A. Formulation of Paramp Gain Characteristics

An equivalent circuit of a parametric amplifier with a double-tuned signal circuit is shown in Fig. 4. In this equivalent circuit, the series resistance of the varactor diode at the signal frequency is neglected for simplicity. The gain response of this paramp is given as follows [4].

$$\frac{G}{G_0} = \frac{1 + (B/A)\alpha^2 + (C/A)\alpha^4 + (D/A)\alpha^6}{1 + (B/E)\alpha^2 + (C/E)\alpha^4 + (D/E)\alpha^6}. \quad (8)$$

Here,

$$G_0 = (A/E), \text{ the gain at the signal center frequency} \quad (9)$$

$$A = [2\sqrt{G_0}/(\sqrt{G_0} + 1)]^2 \quad (10)$$

$$B = [\gamma_A^2 + 2(\gamma_A^2 - X_s)q^2 + (1 - X_s)^2 q^4]/q^2 \quad (11)$$

$$C = X_s^2 + \gamma_A^2 - 2X_s(1 - X_s)q^2 \quad (12)$$

$$D = X_s^2 q^2 \quad (13)$$

$$E = [2/(\sqrt{G_0} + 1)]^2 \quad (14)$$

$$\gamma_A = R_a/R_g = (\sqrt{G_0} - 1)/(\sqrt{G_0} + 1), \text{ the normalized negative resistance of the pumped varactor} \quad (15)$$

$$q = \sqrt{(f_1/f_2)(Q_{u2}/Q_{L1})} \quad (16)$$

$$X_s = (f_2/f_1)(Q_s/Q_{u2})(R_a/R_g) \quad (17)$$

$$\alpha = Q_{L1}q(2\Delta f_1/f_1) \quad (18)$$

and

Q_{L1} loaded Q of the signal resonator
Q_s loaded Q of the second signal resonator.

Under a large-gain condition, (8) becomes

$$\frac{G_0}{G} = 1 + (B/E)\alpha^2 + (C/E)\alpha^4 + (D/E)\alpha^6. \quad (19)$$

From (19), it is understood that paramps with a double-tuned signal circuit may have triple-tuned gain characteristics. The solution to $(d/d\alpha)(G_0/G) = 0$ determines the nature of the paramp gain characteristics, that is, single-tuned or double-tuned or maximally flat or triple-tuned. Under the condition $D/E > 0$, the dependence of the paramp gain characteristic shape on the coefficients in (19) are shown in Table I. In the preceding discussion, single-tuned, or double-tuned, or triple-tuned gain characteristics means that passband gain peaks are one, or two, or three, respectively, and their levels are not necessarily equal.

It is difficult to analytically determine the relations between conditions in Table I and practical paramp parameters. Equations (8)–(18) establish the paramp gain characteristic shape in terms of:

1) the center frequency gain G_0,
2) parameter q which is a function of the ratio of the signal frequency f_1 to the idler frequency f_2, and

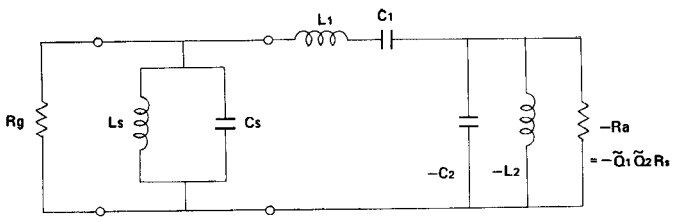

Fig. 4. Signal frequency equivalent circuit of paramp with double-tuned signal circuit.

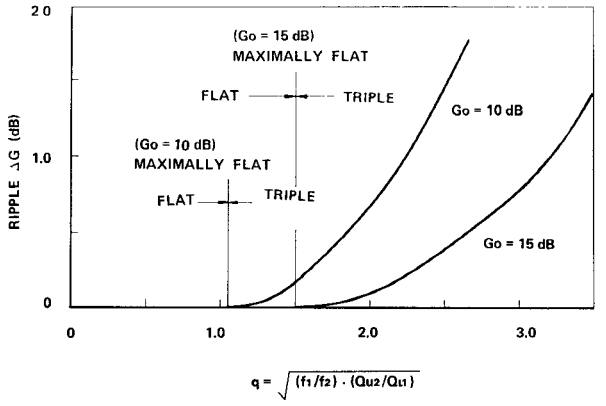

Fig. 5. Gain response shape and ripple level versus paramp parameter q.

TABLE I
RELATIONSHIP BETWEEN GAIN CHARACTERISTICS AND COEFFICIENTS OF GAIN EQUATION

	$C<0$	$C=0$	$C>0$
$B<0$	D.T.	D T	D.T.
$B=0$	D.T	M F	D.T
$\frac{C^2}{3D}>B>0$	T T.	S.T	S.T
$B=\frac{C^2}{3D}$	D.T	S.T.	S.T.
$B>\frac{C^2}{3D}$	S T	S.T	S T

S T : SINGLE TUNED
M F : MAXIMALLY FLAT
D.T : DOUBLE TUNED
T.T : TRIPLE TUNED

that of the unloaded Q of the idler resonator Q_{u2} to the loaded Q of the signal resonator Q_{L1},

3) parameter X_s which is a function of the ratio of the loaded Q of the second signal resonator Q_s to the unloaded Q of the idler resonator Q_{u2}.

Accordingly, the gain response shapes represented by (8) are numerically calculated in terms of G_0, q, and X_s, and the dependence upon these parameters of the paramp gain characteristics has been established.

B. Dependence of Gain Characteristics Upon Paramp Parameters

Numerical calculations indicate that a triple-tuned equiripple gain characteristic can be realized. Fig. 5

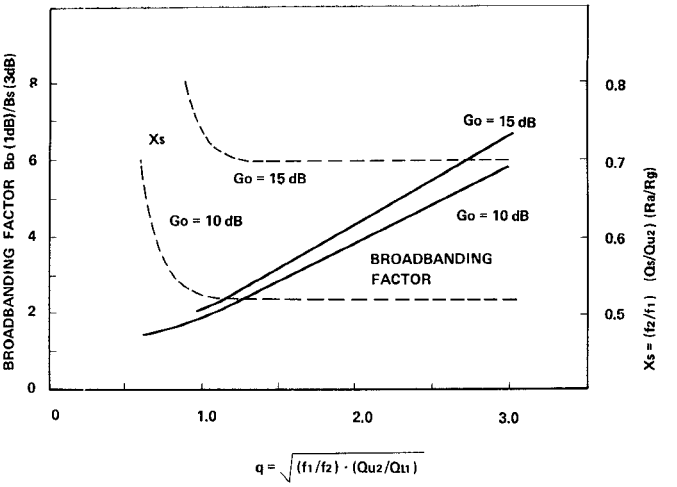

Fig. 6. Broad-banding factor and normalized double-tuning selectivity versus paramp parameter q.

presents the requirement on parameter q in order to obtain monotonic, maximally flat, or triple-tuned equiripple gain characteristics and the corresponding level of gain ripple for the latter case. The required value of parameter q to obtain maximally flat gain characteristics at any gain level has been given [4] by

$$q^2=\frac{\sqrt{G_0}-1}{2}. \tag{20}$$

For midband gains of 10 and 15 dB, the corresponding values of q for maximal flatness become 1.05 and 1.5, respectively, as shown in Fig. 5. For values q smaller than the above, monotonic flat gain characteristics can be obtained and, for those of q larger than the above, triple-tuned equiripple gain characteristics are obtainable. In the latter case, the level of gain ripple becomes larger as q increases and G_0 decreases, respectively.

C. Requirements on Second Signal Resonator Q

The required Q of the second signal resonator corresponding to the gain responses depicted in Fig. 5 is presented in Fig. 6. From these results, the following can be concluded.

1) The required Q of the second signal resonator for triple-tuned equiripple gain characteristics is independent of parameter q and is nearly equal to that required [4] for maximally flat gain characteristics as obtainable from

$$X_s=\frac{\sqrt{G_0}-1}{\sqrt{G_0}+1}. \tag{21}$$

2) The absolute value Q_s representing the required Q of the second signal resonator is independent of midband gain for maximally flat and triple-tuned gain characteristics. For example, the required value of X_s for gains of 10 and 15 dB and the corresponding normalized nega-

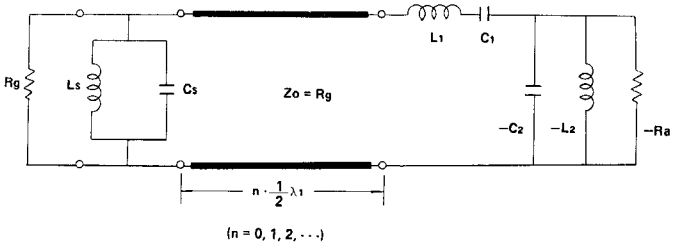

Fig. 7. Paramp signal frequency equivalent circuit including a distributed line between the first and second signal resonators.

tive resistances r_A (15) are 0.52 and 0.70, respectively. Therefore, the following relationship for Q_S/Q_{u2} is valid, for maximally flat and triple-tuned equiripple gain characteristics:

$$\frac{Q_s}{Q_{u2}} \fallingdotseq \frac{f_1}{f_2} . \tag{22}$$

D. Broad-Banding Factor

A broad-banding factor, defined by the ratio of the 1-dB bandwidth obtained with a double-tuned signal circuit to the 3-dB single-tuned bandwidth, is also presented in Fig. 6. It is seen therein that this broad-banding factor increases both with increasing q and G_0.

E. Effects of Line Length Between First and Second Signal Resonator

Concerning the effect of the position of the second signal resonator on bandwidth, previous discussion [10] has indicated that line length between the first and second signal resonators raises the Q of the former. However a more exact investigation is required to determine its effect.

Fig. 7 shows an equivalent circuit for a paramp with a double-tuned signal circuit, including the effect of line length between signal resonators, and neglecting signal frequency series resistance. The latter assumption will not have serious effects for $R_s \ll R_a$.

For a line length of $(n\lambda_1/2)$ $(n=0, 1, 2, \cdots)$, the paramp gain is given by

$$G = \left| \frac{\dfrac{1 - Q_s\Delta \cdot n\pi(\Delta/2) - jn\pi(\Delta/2)}{1 - j(Q_s\Delta + n\pi\Delta/2)} - j\dfrac{Q_{u1}\Delta}{r_g} + r_A \dfrac{1}{1 + jQ_{u2}\Delta(f_1/f_2)}}{\dfrac{1 - Q_s\Delta \cdot n\pi(\Delta/2) + jn\pi(\Delta/2)}{1 + j(Q_s\Delta + n\pi\Delta/2)} + j\dfrac{Q_{u1}\Delta}{r_g} - r_A \dfrac{1}{1 + jQ_{u2}\Delta(f_1/f_2)}} \right|^2 . \tag{23}$$

Here,

λ_1 guide wavelength at f_1
Δ $= 2\Delta f_1/f_1$
r_g $= R_g/R_s$
Q_{u1} unloaded Q of the signal resonator.

Expressing (23) in the same form as (8), computer calculations are performed for the specific case $n=0$, 1, 2, and $Q_{L1}=3$ and 9.

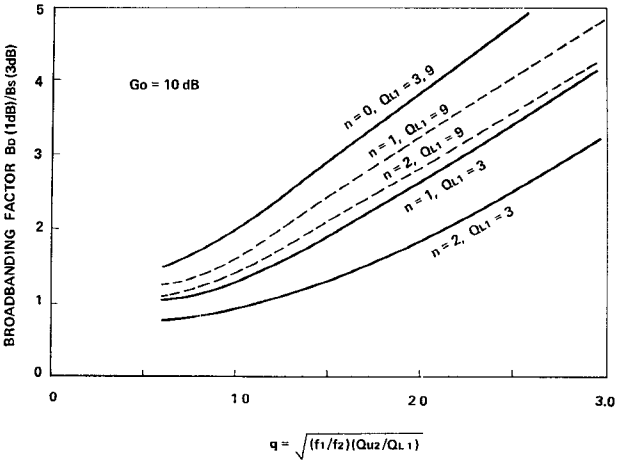

Fig. 8. Broad-banding factor versus paramp parameter q, considering the line length effect.

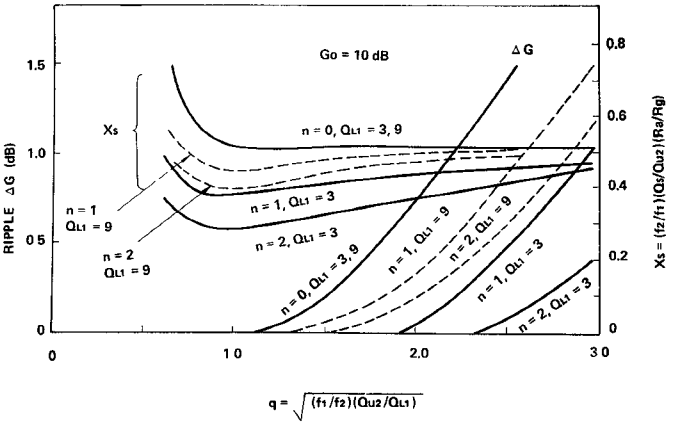

Fig. 9. Gain response shape, ripple level, and normalized double-tuning selectivity versus paramp parameter q and signal line length.

Fig. 8 shows the relation between q and the broad-banding factor for these values.

Fig. 9 presents the gain ripple level of triple-tuned equiripple gain response and normalized parameter X_s as functions of q for the above values of n and Q_{L1}, leading to the following conclusions.

1) The value of n significantly affects the gain response shape, with the value of q required for maximally flat gain characteristics becoming larger with increasing n.

2) For a triple-tuned equiripple gain characteristics, the gain ripple level becomes larger with decreasing n.

3) In the case of both the maximally flat and triple-tuned equiripple gain characteristics, the Q of the second signal resonator is now a function of q for $n \geq 1$.

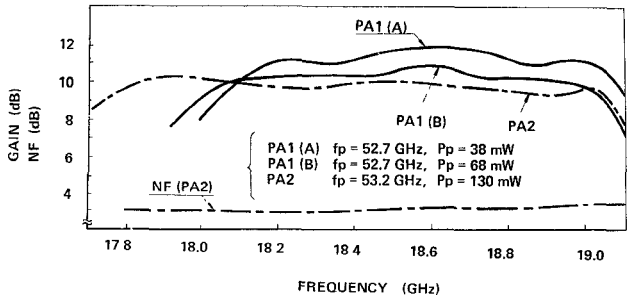

Fig. 10. Measured gain characteristics of 18-GHz paramps.

TABLE II
CALCULATED AND MEASURED VALUES OF WIDE-BAND PARAMP GAIN CHARACTERISTICS

	n	CALCULATED VALUE				MEASURED VALUE
		B_0(1dB) / B_s(3dB)	B_0(1dB) (MHz)	RIPPLE (dB)	Q_s	B_0(1dB) (MHz)
PA1*	0	4.8	1800	1.4	27	—
PA2**	1	3.5	1400	0.5	20	1300
PA1*	2	2.7	1020	0.2	22	830~880

* B_s(3dB) = 380 MHz ** B_s(3dB) = 400 MHz

F. Experimental Results

Several experiments on 18-GHz paramps were carried out and are compared with the preceding theory. A paramp (PA1) utilizing a radial line idler cavity of uniform height equal to that of the miniature pill prong varactor diode used therein, exhibited a single-tuned 3-dB bandwidth of 380 MHz at 10-dB gain. From this bandwidth and the measured $Q_{L1}(=4.2)$, Q_{u2} can be calculated using (24), leading to $q=2.5$:

$$\sqrt{GB} = \frac{2}{(Q_{L1}/f_1) + (Q_{u2}/f_2)}. \tag{24}$$

Gain characteristics obtained with the double-tuned signal circuit are calculated from Figs. 8 and 9 and the results shown in Table II for $n=0$ and 2. For either value of n, triple-tuned gain characteristics are obtained.

In another type of paramp (PA2) utilizing a reentrant idler cavity, the measured single-tuned bandwidth was 400 MHz at 10-dB gain. In the same way as previously described, q becomes 2.5 based upon determination $Q_{L1}(=3.6)$, the single-tuned bandwidth and Q_{u2}. Theoretical gain characteristics obtained using the double-tuned signal circuit and for $n=1$ are also shown in Table II.

The measured gain characteristics exhibited by PA1 and PA2 using a double-tuned signal circuit in each are shown in Fig. 10. For two adjustments of PA1, the second signal resonator is a stub type connected at position $n=2$ and, for PA2, the second signal resonator is an in-line type connected at position $n=1$. It is verified that triple-tuned gain characteristics have been realized using the double-tuned signal circuit, and measured bandwidth has become wider as the position of the second signal resonator is brought closer to the varactor diode. In Table II, experimental results are compared with theory. A maximum bandwidth of 1300 MHz is obtained in PA2 at a gain of 10 dB.

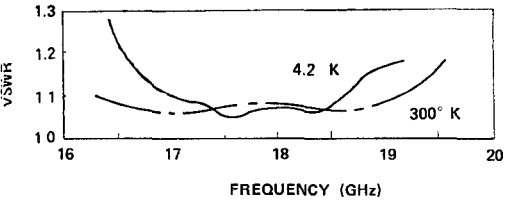

Fig. 11. VSWR characteristics of 18-GHz coaxial circulator under both LHe and room-temperature operation.

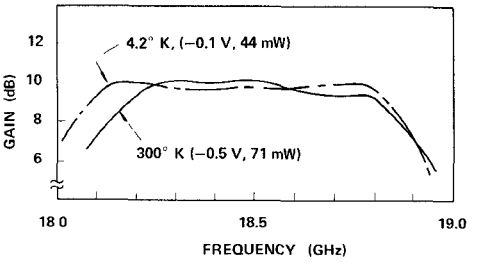

Fig. 12. Measured gain characteristics of 18-GHz paramp under both LHe and room-temperature operation.

IV. PARAMPS PROVIDING BOTH LIQUID-HELIUM- AND ROOM-TEMPERATURE OPERATION

Lithium ferrite is considered to be suitable for the K-band circulator because it has an appropriate value of magnetization and satisfactory temperature characteristics [11]. The temperature dependence of the magnetization has been measured over the temperature range from 373 to 4.2 K [12], resulting in a 10-percent measured variation in magnetization from 300 to 4.2 K.

Using this lithium ferrite, an 18-GHz stripline circulator was constructed and its temperature characteristics measured from 300 to 4.2 K. This circulator includes a quarter-wave transformer on each arm and utilizes 3-mm input and output connectors.

Fig. 11 shows its experimental VSWR characteristics at liquid-helium (LHe) and room temperature measured through a low thermal conductivity waveguide and a waveguide-to-coaxial transition. Its measured insertion losses were 0.3–0.4 dB per path at both temperatures. From these results, it has been possible to ascertain that a circulator capable of both cryogenically cooled and room-temperature operation without any adjustment is realizable.

The gain characteristics of an 18-GHz paramp, using the above mentioned circulator and measured at both room and LHe temperature are shown in Fig. 12. Bias voltage and pump power requirements at room temperature were −0.5 V and 71 mW, respectively. Under LHe cooling, gain characteristics similar to those at room tem-

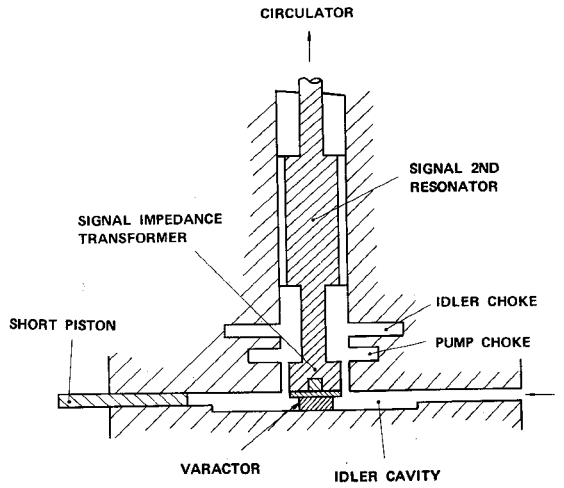

Fig. 13. Cross-sectional view of 18-GHz wide-band paramp.

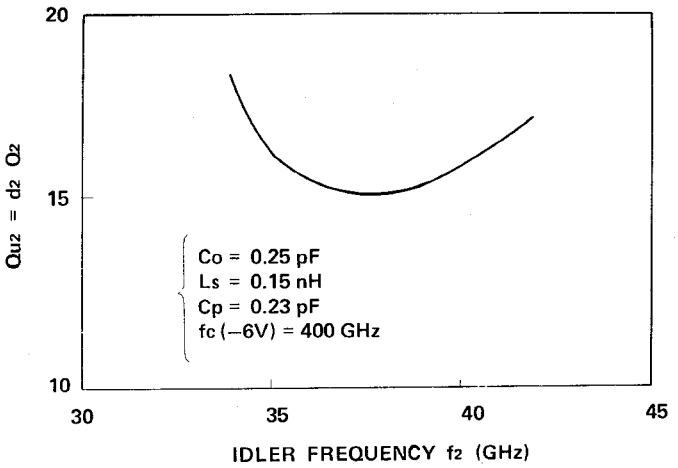

Fig. 14. Calculated value of Q_{u2} versus idler resonance frequency.

perature were obtained, but at bias voltage and pump power settings of -0.1 V and 44 mW, respectively. By virtue of these experiments, it is concluded that paramps operable at both cryogenically cooled and room temperature are feasible.

V. Construction of Paramps

A cross-sectional view of the experimental paramp is shown in Fig. 13. The unloaded Q of the idler resonator, Q_{u2}, is derived assuming that the aperture between the radial line resonator and the signal coaxial line can be ignored.

$$Q_{u2} = d_2 Q_2 = \left\{\frac{1}{2} + \frac{1}{2}\,\omega_2 C_0 \left[\omega_2 L_s + \frac{1}{(\omega_2 C_P + B)^2} \cdot \left(\omega_2 C_P + \omega_2 \frac{\partial B}{\partial \omega}\right)\right]\right\} Q_2. \tag{25}$$

Here,

C_0 junction capacitance of the varactor diode at 0 V,

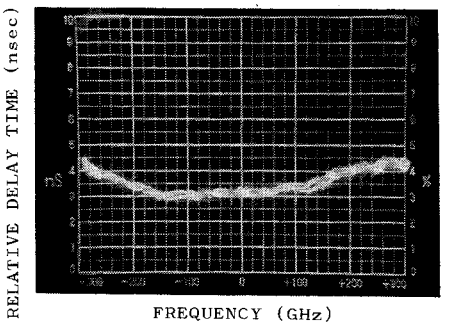

Fig. 15. Relative group delay through 18-GHz low-noise amplifier.

L_s package inductance of the varactor diode,
C_P package capacitance of the varactor diode,
jB susceptance of the radial line resonator, at the outer surface of the varactor diode,
$\partial B/\partial \omega$ susceptance slope of the radial line resonator.

The calculated dependence of Q_{u2} on f_2 shown in Fig. 14 indicates that Q_{u2} becomes a minimum at $f_2 \fallingdotseq 37$ GHz. This frequency is the parallel resonant frequency of the varactor diode.

The second signal resonator may be realized as a stub type and an in-line type element. The in-line type resonator is preferable to the stub type, due to its closer possible proximity to the varactor diode.

VI. 18-GHz Low-Noise Amplifier System

An 18-GHz low-noise amplifier system for the experimental domestic satellite communication earth station has been constructed. It consists of a single stage LHe cooled paramp preceding two stages of room-temperature parametric amplification. The experimental earth station has two receiving frequency bands, 4 GHz and 18 GHz. In all, one 18-GHz paramp stage and three 4-GHz paramp stages are cryogenically cooled with one LHe refrigerator to make the overall low-noise amplifier system simple, small size, and economical.

The measured overall characteristics of the system, including the effect of an input waveguide switch, obtained over the 18.1–18.8-GHz range, included 30-dB gain, ± 0.5-dB gain flatness, 88–100 K noise temperature, and relative group delay variation of 1.5 ns, the latter shown in Fig. 15.

Operation of the first stage paramp at room temperature yields overall noise temperatures of 500–660 K. The calculated noise temperatures of the LHe cooled paramp at cryogenically cooled and room temperature are 23 and 394 K, respectively, and measured noise temperatures near these values are obtained from the measured overall noise temperature.

VII. Conclusion

The design and development of K-band paramps with a double-tuned signal circuit has been discussed in accordance with the following factors. The optimum idler frequency for minimum noise performance decreases upon inclusion of the varactor diode skin effect.

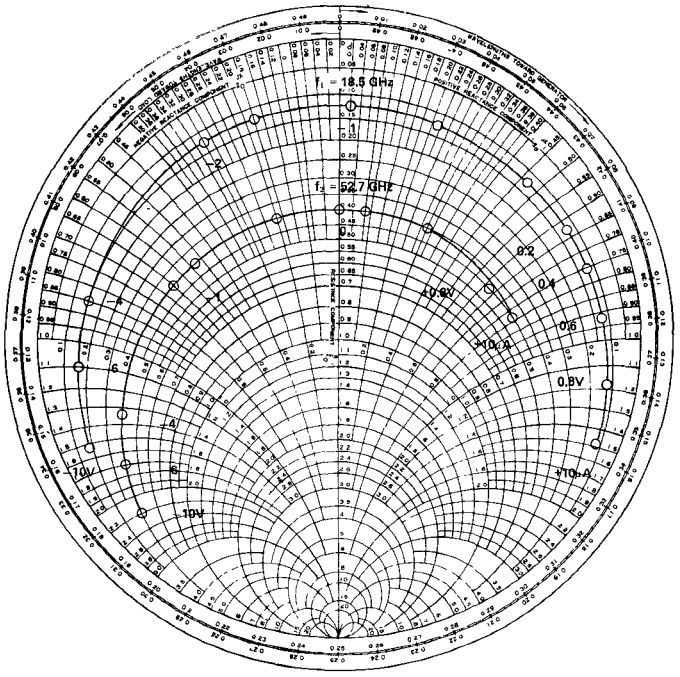

Fig. 16. Measured impedance loci of a mounted varactor versus bias voltage at 18.5 and 52.7 GHz.

It has been shown that triple-tuned equiripple gain characteristics can be realized in paramps utilizing a double-tuned signal circuit. The broad-banding factor, that is, the ratio of the 1-dB bandwidth obtained with the double-tuned signal circuit to the 3-dB bandwidth obtained with a single-tuned signal circuit, has been derived. In this regard, it has been shown that the farther the position of the second signal resonator from the varactor diode, the smaller the broad-banding factor, and that this position also affects the shape of the gain characteristics. The above derivations have been ascertained experimentally.

Using lithium ferrite, a stripline circulator with extremely good temperature characteristics has been developed. With this circulator, an 18-GHz paramp capable of both LHe and room-temperature operation has been realized.

A triple-tuned paramp gain response with a bandwidth of 1300 MHz at a gain of 10 dB has been obtained using a miniature pill prong packaged varactor. Based upon the above theory, it will be possible to obtain a bandwidth larger than 2000 MHz with a varactor having higher parallel resonant frequency than that described above.

Appendix

Influence of Skin Effect on Varactor Diode Q

The series resistance of a GaAs mesa varactor diode at 20 and 50 GHz has been calculated and measured. The resistivity of the p^+ and n^+ layer is estimated as $1\times10^{-3}\,\Omega\cdot$cm, whereas that of the n layer is estimated as $4\times10^{-3}\,\Omega\cdot$cm. Therefore, skin depths at 20 GHz are 11 μm and 22.7 μm, and those at 50 GHz are 6.8 μm and 13.6 μm, respectively. From these values and dimensions of the varactor, the series resistance of the varactor diode at 20 and 50 GHz can be calculated and

$$\frac{R_{S2}(\text{at 50 GHz})}{R_{S1}(\text{at 20 GHz})} = 1.38 = \left(\frac{f_2}{f_1}\right)^{0.36}$$

is obtained.

Fig. 16 shows measured impedance loci of a mounted varactor versus bias voltage at 18.5 and 52.7 GHz [13]. From measured cutoff frequencies at these frequencies,

$$\frac{R_{S2}(\text{at 52.7 GHz})}{R_{S1}(\text{at 18.5 GHz})} = 1.4 = \left(\frac{f_2}{f_1}\right)^{0.32}$$

is obtained.

Generally, an increase of resistance due to skin effect is proportional to $(f_2/f_1)^{1/2}$, but the series resistance of the varactor diode, as shown in the above theoretical and measured estimations, is increased by about $(f_2/f_1)^{1/3}$. Therefore, in this paper, the optimum idler frequency is derived for two cases, $m=2$ and 3.

Acknowledgment

The authors wish to thank Dr. H. Shioya, Nippon Electric Co., Ltd., for his useful comments throughout the duration of the cooperative research project; N. Orime, Mitsubishi Electric Corp., for development of 18-GHz circulators for both LHe and room-temperature operation; and the members of Mitsubishi Electric Corp. for development of the 18-GHz low-noise amplifier system.

References

[1] J. C. Greene and E. W. Sard, "Optimum noise and gain-bandwidth performance for a practical one-port parametric amplifier," *Proc. IRE*, vol. 48, pp. 1583–1590, Sept. 1960.
[2] M. Maeda and A. Sumioka, "Computer-aided design of parametric amplifiers," *IEEE Trans. Microwave Theory Tech.*, vol. MTT-19, pp. 916–921, Dec. 1971.
[3] J. T. DeJager, "Maximum bandwidth performance of a nondegenerate parametric amplifier with single-tuned idler circuit," *IEEE Trans. Microwave Theory Tech.*, vol. MTT-12, pp. 459–467, July 1964.
[4] W. P. Connors, "Maximally flat bandwidth of a nondegenerate parametric amplifier with double tuned signal circuit and single tuned idler circuit," *IEEE Trans. Microwave Theory Tech.* (Corresp.), vol. MTT-13, pp. 251–252, Mar. 1965.
[5] W. J. Getsinger, "Prototypes for use in broadbanding reflection amplifiers," *IEEE Trans. Microwave Theory Tech.*, vol. MTT-11, pp. 486–497, Nov. 1963.
[6] V. Porra and P. Somervuo, "Broadband matching of a parametric amplifier by using Fano's method," *IEEE Trans. Microwave Theory Tech.* (Corresp.), vol. MTT-16, pp. 880–882, Oct. 1968.
[7] K. Kurokawa and M. Uenohara, "Minimum noise figure of the variable-capacitance amplifier," *Bell Syst. Tech. J.*, vol. 40, pp. 695–722, May 1961.
[8] H. A. Haus and R. B. Adler, "Optimum noise performance of linear amplifier," *Proc. IRE*, vol. 46, pp. 1517–1533, Aug. 1958.
[9] K. Garbrecht, "Noise limitation in helium-cooled parametric amplifiers," presented at the 1965 Int. Solid-State Circuits Conf.
[10] S. Egami, "Design of wide band parametric amplifiers," in *IECE Nat. Conv. Rec.* (Japan), 1972, p. 653.
[11] D. H. Temme, G. F. Dionne, and W. E. Courtney, "Lithium ferrites for microwave devices," presented at 1971 G-MTT Int. Microwave Symp., Washington, D.C.
[12] H. Kurebayashi, S. Kawabata, and N. Orime, "18 GHz stripline circulator with good temperature characteristics," *Trans. IECE* (Japan), vol. 55-B, no. 2, pp. 68–69, Feb. 1972.
[13] K. Shirahata, D. Taketomi, H. Ikegawa, H. Shioya, T. Okajima, and S. Egami, "Skin effect on Q of varactor diode," *Trans. IECE* (Japan), vol. 54-B, no. 11, pp. 763–764, Nov. 1971.